

A shear instability mechanism for the pulsations of Rayleigh–Taylor unstable model flames

E. P. Hicks[†]

The Department of Astronomy and Astrophysics, University of Chicago, 5640 S. Ellis Avenue, Chicago, IL 60637, USA

Northwestern University, Center for Interdisciplinary Exploration and Research in Astrophysics (CIERA) and the Department of Physics and Astronomy, 2145 Sheridan Road, Evanston, IL 60208, USA

(Received 29 April 2013; revised 5 February 2014; accepted 4 April 2014)

Previous studies have shown that the behaviour of Rayleigh–Taylor (RT) unstable flames depends on the boundary conditions. If the boundary conditions at the domain walls are impermeable/adiabatic or reflecting then the flame assumes a stable parabolic shape. On the other hand, periodic boundary conditions can produce unstable pulsating solutions. In this paper, we explore why periodic boundary conditions allow unstable solutions by showing the results of two-dimensional direct numerical simulations of model flames. We show that RT unstable premixed model flames pulsate at low gravity because of a shear instability of the vorticity layers behind the flame front. The resulting vortex shedding is controlled by a region of absolute-like instability which moves closer to the flame front as gravity is increased, ultimately disturbing the flame and leading to pulsations. We demonstrate that this region is ‘absolutely unstable’ by showing that the wake is dominated by pure frequency oscillations. In addition, the shear instability can be described by the Landau equation and can be represented dynamically by a Hopf bifurcation. The applicability of the Landau equation allows the apparently complex spatio-temporal behaviour of the vortex shedding to be described by a simple temporal model with only a secondary spatial dependence. We show that the flame behaviour is analogous to the initial instability downstream of a circular cylinder, which leads to the von Kármán vortex street for large enough values of the Reynolds number.

Key words: absolute/convective instability, flames, shear layers

1. Introduction

Premixed flames are spatial volumes of reaction which convert mixed unburnt fuel into burnt products (ashes). In many cases, the distance over which the burning occurs is small compared with other scales in the problem and the flame can be considered as a thin interface between the fuel and the ashes. Thin flame surfaces are subject to three main instabilities: the Darrieus–Landau (DL) instability (Darrieus 1938; Landau 1944), the Rayleigh–Taylor (RT) instability (Rayleigh 1883; Taylor 1950) and thermo-diffusive instabilities. Thermo-diffusive instabilities will not be discussed here; for a general review of flame instabilities see Matalon (2007). The

[†] Email address for correspondence: eph2001@columbia.edu

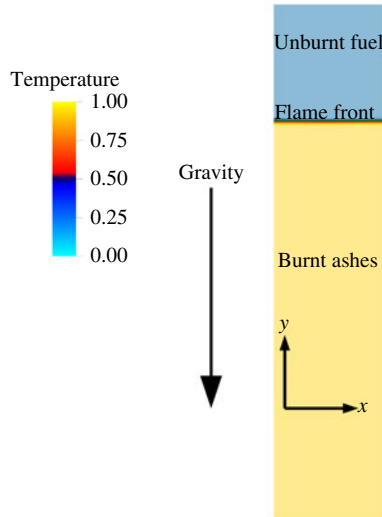


FIGURE 1. A simulation of a laminar flame. Blue represents unburnt fuel and yellow represents burnt ashes. The fuel is more dense than the ashes, so the flame is RT unstable. The flame propagates in the y -direction, opposite to the direction of gravity. The sidewalls have periodic boundary conditions.

DL instability is a fundamental instability of the flame front – the flame is unstable because the fuel expands as it burns, causing a change in density across the flame surface. The flame is also unstable if it propagates upwards against the direction of gravity because, in general, the interface of a more dense fluid above a less dense fluid in a gravitational field is RT unstable. Here, the fuel is more dense than the ashes so the criteria for an RT instability are fulfilled.

Both the DL and RT instabilities disturb what would otherwise be a planar laminar flame (see figure 1). A simple model laminar flame propagates at a characteristic laminar speed (s_o) and with a laminar width (δ), which are determined by the thermal diffusivity of the burning fluid (κ) and the time scale of the reaction ($1/\alpha$, where α is the reaction rate). However, when the flame front is sufficiently perturbed by either the DL or RT instabilities the flame surface is deformed into a new non-planar shape. For both DL and RT unstable flames in rectangular domains or tubes, the flame is often a stable parabola connected to a cusp. The convex part of the parabola points towards the fuel and the cusp points into the ashes (see the temperature field in figure 2). The basic reason for the stabilization of these cusp shapes was suggested by Zeldovich *et al.* (1985): because the flame surface propagates according to Huygen's principle, convex sections of the flame front grow larger and concave sections become smaller, eventually forming a cusp. Under the right circumstances, the final result is a convex parabolic flame front with a cusp.

For the DL instability, the cusp shape and its stability have been the subject of many studies. The basic DL linear stability analysis predicts that the smallest perturbed wavelengths grow the fastest, implying that the instability should grow without bound and lead to a 'self-turbulized' flame with no stabilized shape. However, diffusive processes of the scale of the flame width can limit the growth of these small-scale perturbations. This effect was taken into account phenomenologically by Markstein (1964) and then more rigorously by Clavin & Williams (1982), Pelce &

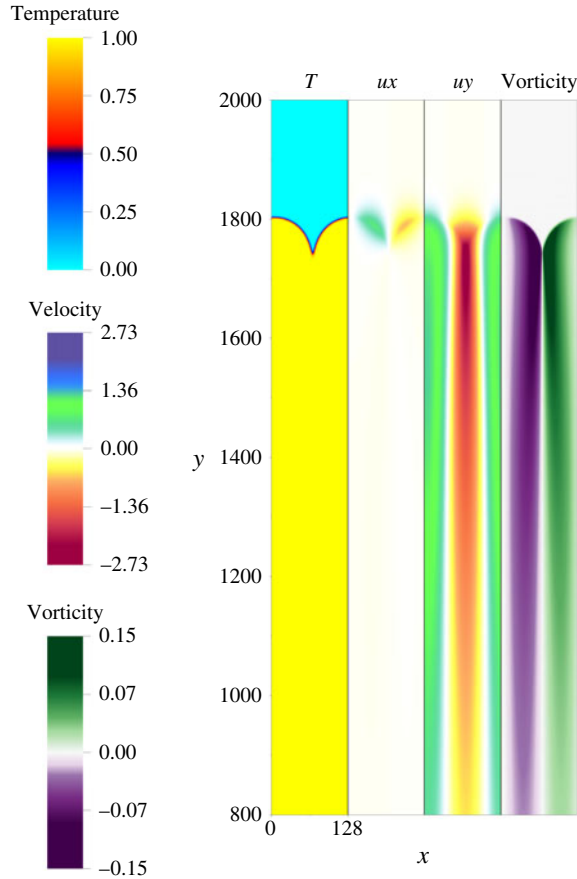


FIGURE 2. Stable rolls, $G = 0.17$. Two stable vorticity rolls extend behind the flame front. In this figure, only part of the computational domain is shown; the actual domain extends from $y = 0$ to $y = 2304$. The temperature field shows that the flame front is parabolic with a cusp near the centre of the domain. This same basic shape is also seen if the boundary conditions are reflecting. The shifting velocity, $v_{shift} = -1.548$, has been subtracted from the y -velocity field to give the y -velocity in the laboratory frame. Here, $G = 0.17$ is the starting condition for the simulations above G_{cr} .

Clavin (1982), Matalon & Matkowsky (1982) and Matalon, Cui & Bechtold (2003). The nonlinear evolution of the DL instability and its stabilization into cusped flames were studied by Michelson & Sivashinsky (1977) and Sivashinsky (1977), who developed a quasilinear parabolic differential equation (the MS equation) for the behaviour of the flame front under the assumption that the thermal expansion across the flame front is small. The MS equation was solved analytically by Thual, Frisch & Hénon (1985) using pole decomposition and these solutions were further studied by Vaynblat & Matalon (2000a,b) and Guidi & Marchetti (2003). The final result of these studies is that one stable steady coalescent pole solution exists and that this solution corresponds to a stably propagating convex flame with a cusp. This work was numerically extended to include realistic density changes across the flame by Rastigejev & Matalon (2006) and to include realistic hydrodynamic strain effects by Creta & Matalon (2011). These papers show that the flame behaviour is dominated

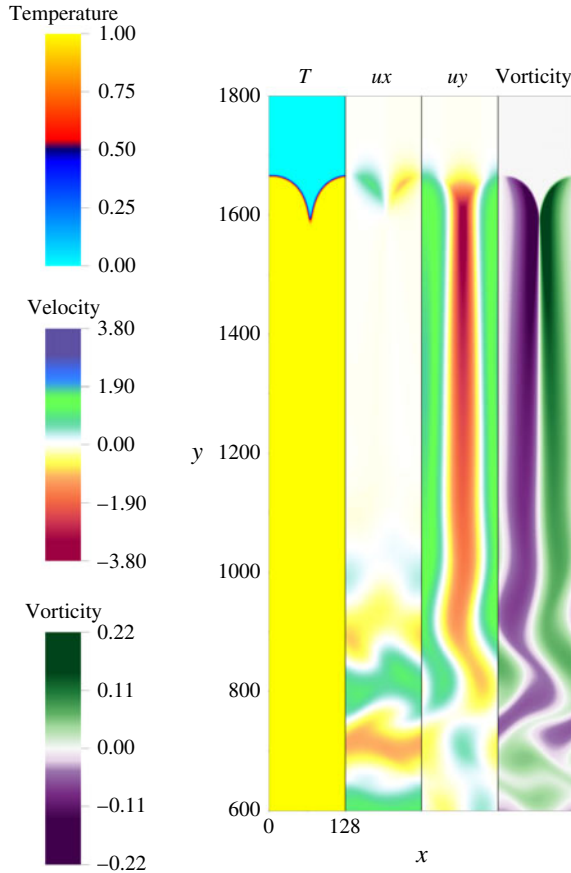


FIGURE 3. Unstable rolls, $G = 0.24$. The vorticity rolls downstream of the flame front are unstable to a shear instability and vortex shedding begins far from the flame front. In this figure, only part of the computational domain is shown; the actual domain extends from $y = 0$ to $y = 2304$. The shifting velocity, $v_{shift} = -1.730$, has been subtracted from the y -velocity field.

by cusps that are stable but also numerically sensitive, implying that the flame might be driven into a turbulent state by background noise.

For the RT instability, the existence of a stable solution for small thermal expansion across the flame front has been similarly established. In the RT case, small thermal expansion only results in a small change in density across the flame front and so the Boussinesq approximation can be applied. Rakib & Sivashinsky (1987) carried out an analysis similar to the Michelson–Sivashinsky analysis of the DL instability to derive a quasilinear parabolic differential equation, the Rakib–Sivashinsky (RS) equation, for the perturbation of a flame front in a cylindrical channel. For a flame propagating in the y direction in a rectangular channel with walls at $x = 0$ and $x = L$, the non-dimensionalized form of this equation is (Berestycki, Kamin & Sivashinsky 2001)

$$\Phi_t - \frac{1}{2}\Phi_x^2 = \epsilon\Phi_{xx} + \Phi - \langle\Phi\rangle, \quad (1.1)$$

where $y = \Phi(x, t)$ is the deviation of the flame profile from flat at a given time, $\langle \Phi \rangle$ is the average profile in the x -direction, $\Phi_{xx} = \partial^2 \Phi / \partial x^2$ and ϵ is a small parameter that depends inversely on gravity. The walls of the channel are impermeable ($u_x(0) = u_x(L) = 0$, where u_x is the velocity in the x -direction) and adiabatic ($\Phi_x(0, t) = \Phi_x(0, L) = 0$). Mikishev & Sivashinsky (1993) numerically demonstrated that for small enough values of ϵ this equation has a dynamically metastable solution that slowly decays to a stable solution. The metastable solution for the interface has a parabolic profile, convex towards the fuel, with the apex (tip) of the parabola near the centre of the channel. The apex of the parabola moves slowly towards the wall and finally meets it, reaching the stable solution. These stable profiles were also observed in simulations of the fluid equations with chemical kinetics by Bychkov *et al.* (1996) and Bychkov & Liberman (2000). The existence and dynamics of the metastable and stable profiles were rigorously proven for a one-dimensional interface by Berestycki, Kamin & Sivashinsky (1995), Sun & Ward (1999), Berestycki *et al.* (2001) and Kamin *et al.* (2005), who transformed the RS equation into a Burgers-type equation. These results were extended to a two-dimensional interface by Berestycki *et al.* (2004). A different transformation of the equation was used by Ou & Ward (2006) and Cheviakov & Ward (2007) to relate the RS equation to the Carrier problem and transform the interface into the spike-layer solution of a singularly perturbed quasilinear parabolic equation for both one-dimensional and two-dimensional interfaces. The overall picture produced by these studies is that RT unstable flames in channels are either stable or nearly stable – the flame is either flat (the laminar solution), or parabolic with the parabola tip near the centre of the channel (the metastable solution) or parabolic with the tip on the channel wall (the stable solution). Unlike the MS equation, no cusped solutions exist (a direct comparison of the RS equation and the MS equation can be found in Guidi & Marchetti (2003)). The adiabatic boundary conditions on the flame profile force the interface to be perpendicular to the walls which prevents cusp formation at the walls. No cusp forms between the walls because the parabolic solution holds.

However, other boundary conditions, reflecting and periodic, produce different results in reacting flow simulations. Reflecting boundary conditions effectively keep the wall impermeability condition used in the derivation of the RS equation, but replace the adiabatic temperature condition so that the flame profile no longer must be perpendicular to the wall. Specifically, $u_x(x_{wall} + x) = -u_x(x_{wall} - x)$, $u_y(x_{wall} + x) = u_y(x_{wall} - x)$ and $T(x_{wall} + x) = T(x_{wall} - x)$, where x is the spanwise coordinate, x_{wall} is the position of the wall, u_x is the spanwise velocity and u_y is the streamwise velocity. The resulting solution appears to be mirrored with respect to the boundary. These conditions were used by Vladimirova & Rosner (2003) for Boussinesq simulations of an RT unstable model flame. They studied the flame behaviour while varying two parameters: $G = g(\Delta\rho/\rho_o)\delta/s_o^2$, where g is the gravitational acceleration, ρ_o is the density of the unburnt material and $\Delta\rho$ is the change in fluid density across the flame front, and $L = \ell/\delta$, where ℓ is the domain size. For a given L , when G is small, the flame is laminar (see figure 1) and the flame speed is equal to the laminar flame speed, s_o . When G exceeds a critical value, G_1 , an apparently stable parabolic solution with a cusp-like feature between the walls appears (see figure 2). This numerical solution looks very similar to the analytical solution of the RS equation, except for the existence of the cusp. Two vorticity rolls extend downstream of the flame surface (see figure 2). This vorticity is produced by temperature gradients in the spanwise direction (here, the x -direction), in other words, by deviations of the flame surface from flat. The cusped flame moves

faster than the laminar flame, but its speed is constant because the flame front is not changing shape and, in general, the flame speed is proportional to the flame surface area (Damkohler 1940 (trans. 1947)). To summarize, simulations show that reflecting boundary conditions produce a cusped flame which propagates with a constant speed as a travelling wave. However, these properties have not yet been established analytically.

Simulations using periodic boundary conditions on the sidewalls show different flame morphologies for both impermeable/adiabatic and reflecting boundary conditions. Periodic boundary conditions are the most often used for simulations of RT unstable flames. These conditions relax both the impermeability and adiabatic conditions on the walls and the result is a flame of very different nature from the stable travelling wave seen in both the solutions of the RS equation and simulations with reflecting boundary conditions. This was first noted by Vladimirova & Rosner (2005), who showed that periodic boundary conditions give different results from reflecting boundary conditions (Vladimirova & Rosner 2003). In this comparison, reflecting boundary conditions led to a stable flame shape while periodic boundary conditions yielded a ‘pulsating’ unstable flame with an oscillating flame speed (see figure 3). They suggested that the regular travelling wave solution for a cusped flame in a periodic domain is only metastable and that, if the travelling wave is perturbed, it will inevitably develop into a pulsating wave solution.

The fact that unstable pulsating solutions can develop when the wall boundary conditions are periodic is of key importance to understanding the behaviour of RT unstable flames in Type Ia supernovae. To understand the timing, nuclear products and fundamental explosion mechanism of Type Ia supernovae, astronomers need an accurate understanding of RT unstable flames, including whether they can be disturbed by any turbulence that they create. This understanding is also needed to develop appropriate subgrid models for large full-star simulations of these explosions. The effect of self-generated turbulence on RT unstable flames is often studied by simulating the flames in isolation (Khokhlov 1995; Vladimirova & Rosner 2003; Bell *et al.* 2004; Vladimirova & Rosner 2005; Zingale *et al.* 2005; Zhang *et al.* 2007; Chertkov, Lebedev & Vladimirova 2009; Hicks & Rosner 2013). However, supernova flames are essentially unconfined, so the choice of boundary conditions imposed in the simulations is problematic. The solution, so far, has been to use periodic boundary conditions to approximate an unconfined domain. However, the size of the domain limits the regimes that can be studied. Researchers often either study the initial transient behaviour of the flame (which is sensitive to the initial conditions) or study a final statistically-steady saturated state, in which the growth of the RT instability is limited by the domain size. Ideal simulations that pass the initial phases of growth but do not saturate are computationally expensive due to the required range of scales. In any case, an understanding of the types of solutions allowed by the periodic boundary conditions is necessary to understand the current body of simulation results and may eventually lead to a better understanding of the unconfined case. The aim of this paper is to explain why flames in simulations with periodic boundary conditions are unstable and pulsating instead of the stable travelling waves observed when the boundary conditions are either impermeable/adiabatic or reflecting.

In this paper, we will show that the unstable pulsations observed under periodic boundary conditions are actually caused by a shear instability of the vorticity rolls downstream of the flame front. In our simulations of periodically bounded RT unstable model flames, we observe several behaviour regimes as the non-dimensional gravity, G , is increased. Above G_1 , at which the cusped solution develops, there is a range

of G values for which the travelling wave solution is entirely stable, as in the case of reflecting boundary conditions. At a critical value, G_{cr} , a shear instability of the vorticity rolls begins in a region of ‘absolute instability’ far behind the flame front. An absolutely unstable region is controlled by a local instability which amplifies a pure frequency in such a way that it is not carried away by the flow, but resonantly reinforces itself (Huerre & Monkewitz 1985). We will show that the onset of this instability is well-described by the Landau equation and therefore can be represented by a Hopf bifurcation as G_{cr} is exceeded. After pure-frequency modes grow in the region of absolute instability, they are carried downstream as shed vortices by a region of convective instability. For higher values of G , the region of absolute instability is located closer to the flame front until, when G is large enough, the instability region is close enough to disturb the flame itself. It is this interaction between the region of instability and the flame front that causes the flame to pulsate.

The initial shear instability of the rolls is similar to the initial development of the von Kármán vortex street downstream of a circular cylinder, analysed by Strykowski (1986), Provansal, Mathis & Boyer (1987), Sreenivasan, Strykowski & Olinger (1987) and Strykowski & Sreenivasan (1990). We follow their approach closely by modelling the onset of the instability with the Landau equation and as a Hopf bifurcation. The physical picture of a region of ‘absolute instability’ some distance behind the cylinder (or flame) followed downstream by a region of ‘convective instability’ was also suggested in these papers.

We continue with the details of the numerical simulation set-up in § 2. Then, in § 3, we show that an instability of the vorticity rolls begins far downstream of the flame front. This is followed by a discussion of the Landau equation in § 4, and then measurements from our simulations showing that the roll instability follows this equation in § 5. Finally, we discuss and analyse the results in § 6, showing that the unstable region produces pure modes of oscillation, suggesting that the region is absolutely unstable. We also discuss the Hopf bifurcation with which the instability begins.

2. Problem formulation

To understand the influence of the boundary conditions on RT unstable flames, we simulated a simple model flame problem. Realistic, fully compressible combustion simulations would include mass conservation, momentum conservation, species balance equations, enthalpy conservation and detailed chemistry. Our model includes two major simplifications: the Boussinesq approximation and the use of a model reaction.

The Boussinesq approximation is appropriate for subsonic flows when the density variations in the flow are small. In the approximation, the fluid is governed by the incompressible Navier–Stokes equation with a temperature-dependent forcing term that incorporates the gravitational acceleration. In this model, density differences in the flow appear only in the buoyancy term, which depends, for our case, on the density difference across the flame front, $\Delta\rho$. All other terms depend only on the density of the unburnt material, ρ_o . Therefore, the flame is subject to the RT instability (because buoyancy forces are included), but not the DL instability (because the change in density across the flame front is not considered outside of the buoyancy term). This allows us to isolate the effect of the RT instability on the flame. Using the Boussinesq approximation also allowed direct comparisons with flame shape solutions of the RS equation and with Vladimirova & Rosner (2003, 2005), all of which use the Boussinesq approximation.

Our second simplification is to use a model reaction term, $R(T)$, in an advection–reaction–diffusion equation which describes temperature transport and burning. Here, T is a reaction progress variable that tracks the state of the fluid from a unburnt fuel at temperature $T=0$ to burnt ashes at temperature $T=1$. The reaction progress variable represents both the mass fraction of burned material and the fraction of energy released into the flow (Vladimirova, Weirs & Ryzhik 2006). This simplified treatment of the reaction has been used in many other studies, and there are several possible forms of $R(T)$ including the Kolmogorov–Petrovskii–Piskunov (KPP), m th-order Fisher, bistable, Arrhenius and ignition reactions (for a review of model reaction types see Xin 2000). In this study we chose $R(T) = 2\alpha T^2(1 - T)$, a version of the bistable reaction with the ignition temperature set to zero which, therefore, exhibits no bistable behaviour. We avoided the KPP reaction used by Vladimirova & Rosner (2003, 2005) because of its unstable fixed point at $T = 0$ which makes the reaction numerically unstable for long integrations.

The bistable reaction has a simple laminar solution in a stationary gravity-free fluid (Constantin, Kiselev & Ryzhik 2003). When the flame is laminar, it is completely flat with a characteristic width of δ and it moves with the laminar flame speed s_o . Here, δ and s_o are set by α , the laminar reaction rate, and κ , the thermal diffusivity, such that $s_o = \sqrt{\alpha\kappa}$ and $\delta = \sqrt{\kappa/\alpha}$. The actual flame thickness (δ_t) is larger than the characteristic flame width (δ) by a factor of 4 ($\delta_t = 4\delta$), as calculated by measuring the distance between the level sets $T=0.1$ and $T=0.9$.

The fluid equations were non-dimensionalized by the characteristic length scale (laminar flame front thickness, δ) and time scale in the problem (the reaction time, $1/\alpha$) (Vladimirova & Rosner 2003) to give

$$\frac{D\mathbf{u}}{Dt} = - \left(\frac{1}{\rho_o} \right) \nabla p + GT + Pr \nabla^2 \mathbf{u}, \quad (2.1a)$$

$$\nabla \cdot \mathbf{u} = 0, \quad (2.1b)$$

$$\frac{DT}{Dt} = \nabla^2 T + 2T^2(1 - T) \quad (2.1c)$$

and to yield our first two control parameters

$$G = g \left(\frac{\Delta\rho}{\rho_o} \right) \frac{\delta}{s_o^2}, \quad (2.2)$$

$$Pr = \frac{\nu}{\kappa}, \quad (2.3)$$

where G is the non-dimensionalized gravity and Pr is the Prandtl number. Here, ρ_o is the density of the unburnt fuel and $\Delta\rho$ is the increase in density across the flame front, so that $\rho(T) = \rho_o + \Delta\rho T$. In this formulation, p is the pressure deviation from hydrostatic equilibrium. To simplify the problem, physical characteristic values, such as ν (the kinematic viscosity) and κ , are taken to be constants independent of temperature. Here, G is positive if the flame is moving in the opposite direction from the gravitational force, as is the case here. The non-dimensional box size, $L = \ell/\delta$, is the third and final control parameter. In this set of simulations, $L = 128$ and $Pr = 1$; only G is varied. These parameters can be translated into the densimetric Froude number, $Fr_d = 1/\sqrt{GL}$, and into the ϵ parameter used by Berestycki *et al.* (2001), $\epsilon = 2/GL^2$.

The boundary conditions were periodic on the sidewalls for all the simulations. The top of the simulation domain was subject to an inflow condition with $u_x = 0$ and $u_y = -v_{shift}$. We set v_{shift} equal to the expected average flame speed, which for these simulations was approximately 1.7 in units of the laminar flame speed. The inflow velocity held the flame surface in a nearly fixed reference position within the domain. The bottom of the simulation domain was subject to an outflow condition in which a small region at the bottom of the domain was made compressible so that all characteristics near the bottom of the domain pointed out of the domain. We compared the results from this configuration with simulations in which the bottom boundary was subject to an outflow condition with $u_x = 0$ and $u_y = -v_{shift}$ and found that the bottom boundary condition did not make a difference to the flow away from the boundary. The temperature was held at $T = 0$ (fuel) for the top boundary and $T = 1$ (ash) for the bottom boundary. The flame surface remained within the domain and did not approach either boundary.

The aim of these simulations was to measure the growth of the shear instability in the velocity field downstream of the flame surface. Typically, one begins with a stable configuration (in this case for the flame front and vorticity rolls) and then ‘turns on’ the instability to measure its development. For example, Strykowski (1986), Sreenivasan *et al.* (1987) and Strykowski & Sreenivasan (1990) found that the best way to measure the growth of instabilities in the shear layers behind a cylinder was to increase the value of the Reynolds number (Re) from just below the critical Re up to a target Re for which the flow would be unstable. They began their experiment with Re slightly below the critical Re and then allowed all the perturbations and unsteady behaviour from establishing the flow to decay. Then they quickly increased their flow rate to the target Re and watched the instability develop. This procedure allows the instability to develop cleanly and minimizes the effect of perturbations caused by changing the flow rate. We followed a similar procedure. First, we simulated the flame with $G = 0.17$, which is below the critical G , G_{cr} , for which the shear instability begins. After allowing all perturbations to decay, we were left with a stable cusped flame shape with steady rolls behind it (see figure 2). Next, we used this condition as the starting point for a group of simulations above G_{cr} with values of $G = 0.24, 0.25, 0.26, 0.27, 0.28$ and 0.29 . When these new simulations started, there was still a small increase in the flame cusp length due to the higher G . This shape adjustment created a perturbation that can be seen as the first maximum or minimum in the time series data, which will be explained in § 5 (for an example, see figure 6).

The flame front in the base simulation at $G = 0.17$ was initially perturbed by a randomly seeded group of sinusoids with an amplitude of 3.0 and wavenumbers between $k_{min} = 4$ and $k_{max} = 16$. The initial temperature profile was given by $T(x, y) = 0.5(1 - \tanh(2r(x, y)/\delta_r))$, where $r(x, y) = y - q(x)$ and where $q(x)$ is the position of the flame front including the effect of the perturbation and δ_r is the initial width of the front, which is $\delta_r = 4$ for the bistable reaction. All other simulations began with the developed stage of the $G = 0.17$ simulation.

The simulations were run for $t = 2004$ with a time step of 0.006 and data were recorded every 2.004. This produced 1000 data points for every velocity time series that we analysed. The simulation domain contained 16 elements in the x -direction and 288 elements in the y -direction, for a total of 4608 elements covering a physical scale of 128×2304 . Each element contained a 14×14 grid of collocation points. We chose this high spectral order to ensure accuracy for the instability measurements. The resolved scale is much below the viscous scale and the flame width.

We verified that our simulations were resolved in two ways. First, the flame speed did not change when lowering the spatial resolution to 8×144 elements. Second, the Landau constants (which will be measured in § 5) also did not change substantially with resolution. Most constants did not change by more than a few per cent between the two resolutions; the largest change was in da_r/dG , which changed by 16 %, due to some change in the overall velocity magnitude of the developing instability for small velocities. We consider this to be acceptable, given the sensitivity of the instability that we are studying.

All simulations used Nek5000 (Fischer, Lottes & Kerkemeier 2008), a freely available open-source highly scalable spectral element code currently developed by P. Fischer (chief architect), J. Lottes, S. Kerkemeier, A. Obabko and K. Heisey at Argonne National Laboratory.

3. The shear instability

In this section, we discuss the general appearance and nature of the shear instability of the vorticity rolls downstream of the flame front. A mathematical model for the onset of the instability (the Landau equation) will be discussed in later sections. Simulations for $G = 0.24$ – 0.29 show that a shear instability develops far downstream of the flame front (see figures 3–5). Visually, the vorticity rolls are straight near the flame front and only begin to bend far downstream of the flame front. The x -velocity is small near the flame front, but horizontal layers begin to develop downstream. For higher values of G , the region of vortex shedding, which is a result of the shear instability, is located closer to the flame front.

One important question is whether the instability is controlled by the flame front or by some region downstream of the flame front. In other words, is this a true shear instability or is this a flame front instability (for example, the RT instability) that is only magnified far downstream? This question can be answered by noting that the flame speed for these simulations is not oscillating, which means that the flame front is not changing shape. This shows that the instability is innate to the shear layers and is not controlled by the flame front. Therefore, the only effect of the RT instability is the development of the stable cusp shape which, in turn, creates the shear layers. These simulations directly show that, even with periodic boundary conditions, stable travelling wave solutions do exist for some values of G , in contrast to the hypothesis of Vladimirova & Rosner (2005) that all such solutions would be metastable. In the next section, we model the development of the shear instability with the Landau equation.

4. The Landau equation

The Landau equation (Drazin & Reid 2004; Landau & Lifshitz 2004),

$$\frac{dA}{dt} = aA - \frac{1}{2}c|A|^2A, \quad (4.1)$$

describes the growth of an instability in a small region of G near G_{cr} . When $G \leq G_{cr}$, no modes are unstable. When G is slightly larger than G_{cr} , the derivation of the Landau equation assumes that one dominant mode of the amplitude parameter, A , is unstable. For this study, we chose the normal velocity, u_x , as A . At first, the amplitude of the dominant mode grows exponentially in time, but eventually the nonlinear interaction of the mode with itself becomes important (Drazin & Reid 2004).

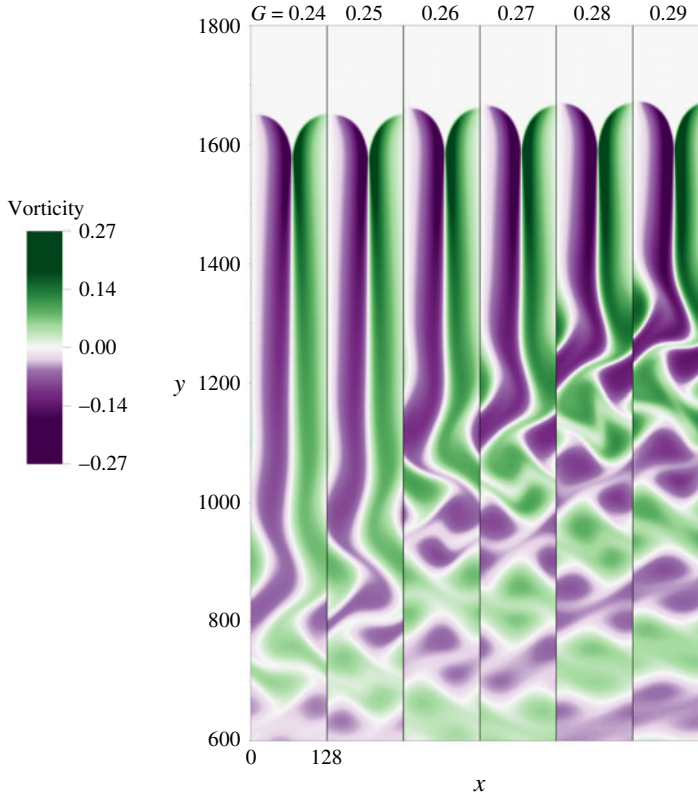


FIGURE 4. The vorticity for $G = 0.24\text{--}0.29$. The vortex shedding region is closer to the flame front for higher values of G . Finally, for high enough G , the vortices are close enough to the flame front to fully disturb it, causing the flame to pulsate. This, in turn, causes the flame speed to oscillate.

Self-interaction causes A to level off to a constant value. For the flame system, we verify that the instability follows the Landau equation and we fit for the Landau constants; however, we do not derive the equation directly.

The Landau equation has two constants, a and c . Both constants can be complex and they depend on G and G_{cr} , so $a(G, G_{cr}) = a_r(G, G_{cr}) + ia_i(G, G_{cr})$ and $c(G, G_{cr}) = c_r(G, G_{cr}) + ic_i(G, G_{cr})$. By choosing the solution $A = u_x = u_o e^{i\phi(t)}$, the Landau equation becomes two equations: one for the amplitude (u_o) and one for the phase (ϕ),

$$\frac{du_o}{dt} = a_r u_o - c_r u_o^3, \quad (4.2a)$$

$$\frac{d\phi}{dt} = a_i - c_i u_o^2. \quad (4.2b)$$

Here, a_r describes the initial exponential growth of u_o , $u_o \propto \exp(a_r t)$; c_r limits this growth at long times and causes u_o to saturate at a constant value, u_{os} . The initial frequency of the oscillations of u_x is given by $a_i/2\pi$ because $d\phi/dt = 2\pi f$, where f is the frequency. Here, c_i changes the frequency for long times. The final, saturated value of the frequency is f_s . In general, a quantity with subscript 's' refers to the saturated value of that quantity.

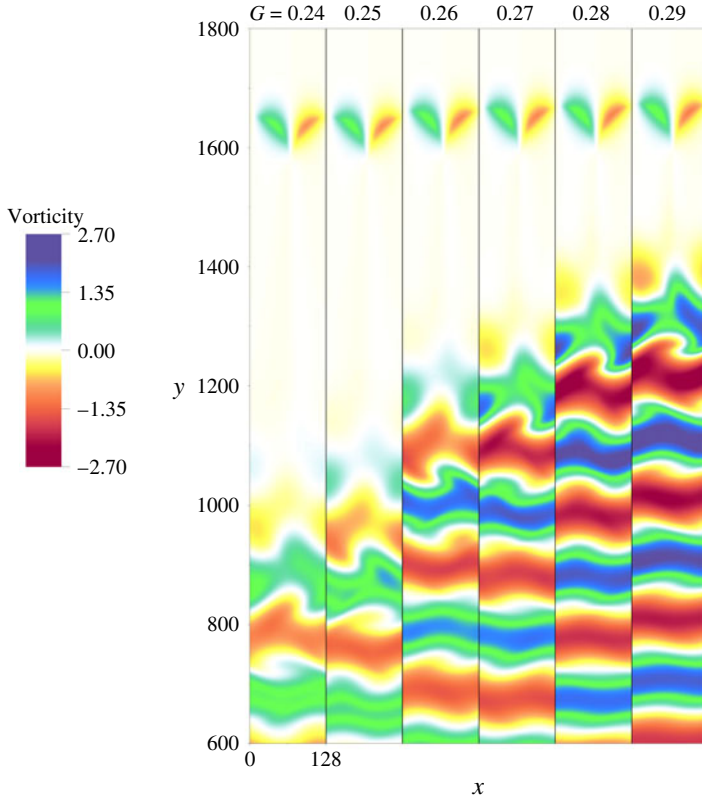


FIGURE 5. The velocity in the x -direction for $G = 0.24$ – 0.29 , corresponding to the vorticity measurements shown in figure 4. Substantial x -velocities only develop downstream of the flame front. We used the x -velocity as the amplitude parameter for the measurements of the constants of the Landau equation.

The Landau equation should be valid for a small region of G just above G_{cr} , so a_r , c_r , a_i and c_i are expanded in Taylor series around G_{cr} ,

$$a_r(G) = \frac{da_r}{dG}(G - G_{cr}) + \dots, \tag{4.3a}$$

$$a_i(G) = a_{io}(G_{cr}) + \frac{da_i}{dG}(G - G_{cr}) + \dots, \tag{4.3b}$$

$$c_r(G) = c_{ro}(G_{cr}) + \frac{dc_r}{dG}(G - G_{cr}) + \dots, \tag{4.3c}$$

$$c_i(G) = c_{io}(G_{cr}) + \frac{dc_i}{dG}(G - G_{cr}) + \dots, \tag{4.3d}$$

where $a_{ro}(G_{cr}) = 0$ by definition. Substitution of these expressions back into the Landau equations yields a set of algebraic equations. These equations depend on the independent variable G and measured knowns $\{a_r, u_{os}, f, f_s\}$, leaving the unknowns

$$\left\{ G_{cr}, \frac{da_r}{dG}, a_{io}, \frac{da_i}{dG}, c_{ro}, \frac{dc_r}{dG}, c_{io}, \frac{dc_i}{dG} \right\} \tag{4.4}$$

to be solved for. The result is the system of equations

$$a_r(G_{cr}) = 0, \quad (4.5a)$$

$$a_r(G) = \frac{da_r}{dG} (G - G_{cr}), \quad (4.5b)$$

$$u_{os}^2 = \left(\frac{da_r}{dG} \right) \frac{1}{c_{ro}} (G - G_{cr}) - \left[\frac{\left(\frac{da_r}{dG} \right) (G - G_{cr})^2 \frac{dc_r}{dG}}{c_{ro}^2 + \frac{dc_r}{dG} (G - G_{cr}) c_{ro}} \right], \quad (4.5c)$$

$$2\pi f_s = a_{io} + \left[\frac{da_i}{dG} - \frac{c_{io}}{c_{ro}} \frac{da_r}{dG} \right] (G - G_{cr}) - \left(\frac{1}{c_{ro}} \right) \frac{da_r}{dG} \frac{dc_i}{dG} (G - G_{cr})^2, \quad (4.5d)$$

$$a_i = a_{io} + \frac{da_i}{dG} (G - G_{cr}), \quad (4.5e)$$

$$2\pi f = a_i - c_i u_o^2, \quad (4.5f)$$

$$c_i = c_{io} + \frac{dc_i}{dG} (G - G_{cr}), \quad (4.5g)$$

$$u_{os} = \left(\frac{a_r}{c_r} \right)^{1/2}. \quad (4.5h)$$

Under the simplifications that $c_i = c_{io} = dc_i/dG = 0$ and $dc_r/dG \approx 0$, the equations become

$$a_r(G_{cr}) = 0, \quad (4.6a)$$

$$a_r(G) = \frac{da_r}{dG} (G - G_{cr}), \quad (4.6b)$$

$$u_{os}^2 = \left(\frac{da_r}{dG} \right) \frac{1}{c_{ro}} (G - G_{cr}), \quad (4.6c)$$

$$2\pi f = a_i = a_{io} + \frac{da_i}{dG} (G - G_{cr}), \quad (4.6d)$$

$$u_{os} = \left(\frac{a_r}{c_r} \right)^{1/2}. \quad (4.6e)$$

Our measurements show that $c_i = 0$, but they are not adequate to definitely prove that $dc_r/dG \approx 0$ (see § 5.2). This does not fundamentally change the character of our results. The point of our measurements is to test these equations, derived from the Landau equation, as a model for the shear instability and, since these equations do provide a good fit, find the Landau constants.

5. Measurement of the Landau constants

5.1. Measurement procedure

This subsection explains how we measured the Landau constants from our simulation data. First, it was necessary to establish a rest frame for the system. For the case of flow past a cylinder, Strykowski and Sreenivasan simply used the rest frame of the cylinder. For the flame system, we used the rest frame of the top of the flame surface. Once the flame has established its final parabolic/cusped shape this frame is also the

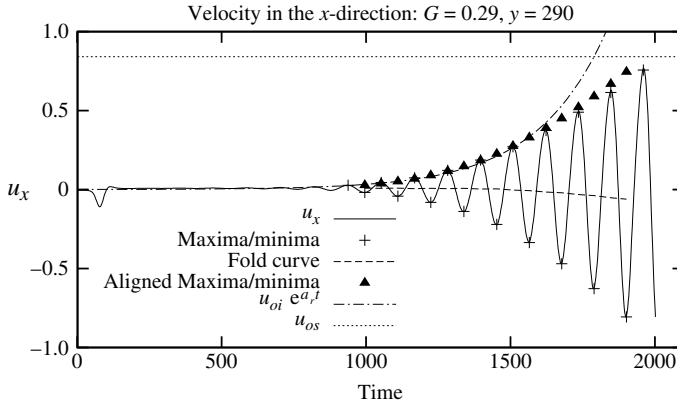


FIGURE 6. An example of the measurement procedure used to find the Landau constants. The velocity in the x -direction, u_x , is measured at a point, creating a time series (solid curve); this particular time series is for $G = 0.29$ at the point $x = 19$, $y = 290$. It should be noted that y is measured from the top of the flame surface. Next, the maxima and minima of the time series are extracted (cross symbols). Because a mean velocity tends to develop, the maxima and minima are aligned with respect to a fold curve (long-dashed line). The absolute values of the aligned maxima and minima (solid triangles) are used to fit for the Landau constants: the exponential growth rate, a_r (fit shown as dot-dashed curve), the saturated velocity, u_{os} (fit shown as short-dashed line) and the period, P (fit not shown). The first minimum in the graph is due to the initial lengthening of the cusp from the $G = 0.17$ stable flame shape.

rest frame of the entire flame. For the rest of the paper, we consider the dynamics in a new coordinate system in which $y = 0$ is at the top of the flame front and y is positive downstream of the flame. In this rest frame, we chose a grid of points at which to measure our amplitude parameter, u_x . This grid had a spacing of $\delta_x = 1$ and $\delta_y = 10$, beginning at $y = 0$ (the top of the flame front) and continuing downstream of the flame front. Then, we measured $u_x(t)$ at each grid point for the duration of the simulation. For each velocity curve, we fitted the data for a_r (the growth rate), u_{os} (the saturated velocity) and P (the period of oscillations). An example of this measurement procedure is shown in figure 6.

There were several difficulties in making these measurements. First, the underlying mean velocity had a tendency to shift slightly away from zero as the instability developed. Our solution was to effectively ‘fold’ the u_x curve around a changing mean value (the ‘fold curve’) to find new aligned maxima and minima of the u_x curve. The outcome of the folding is that the maxima and minima are aligned with respect to $u_x = 0$. The maxima and absolute values of the minima are used together for one fit instead of fitting them separately. Second, limitations on computing time necessarily meant that u_x could not reach u_{os} during the simulation time for some of the grid points. As a result, u_{os} had to be inferred indirectly from the data instead of being measured directly in many cases.

The general measurement procedure is as follows. First, extract the maxima and minima from the graph of u_x . Using the folding method, align these points to make one curve. Next, use a linear fit to find the growth rate, a_r , of the exponential $e^{a_r t}$. We made sure that data from later times, when u_x was beginning to saturate, were deweighted. Now that a_r is known, u_{os} can be found by another linear fit. In fact, the

equation for the amplitude of u_x , that is u_o , can be solved analytically (Provansal *et al.* 1987; Landau & Lifshitz 2004) to give

$$u_o(t) = u_{os} \left[1 + \left(\frac{u_{os}^2}{u_{oi}^2} - 1 \right) e^{-2a_r t} \right]^{-1/2}, \quad (5.1)$$

where u_{oi} is the initial, perturbed velocity. We found that this solution could be manipulated into the form of a straight line with slope u_{os}^2 . By defining $f(t) = e^{-2a_r t}$,

$$\frac{1 - f(t)}{f(t)} = u_{os}^2 \left[\frac{1}{f(t)u_o(t)^2} \right] - \frac{u_{os}^2}{u_{oi}^2}, \quad (5.2)$$

so u_{os}^2 can be easily found from the known quantities $(1 - f(t))/(f(t))$ and $1/(f(t)u_o(t)^2)$.

5.2. The Landau constants

In this subsection, we show measurements of the growth rate, $a_r(G)$, the saturated velocity, $u_{os}(G)$, and the period of oscillations, $P(G)$. From these measurements, we find the Landau constants.

We begin by showing the measurement for a_r and we subsequently deduce G_{cr} and da_r/dG . The results from the growth rate measurements are shown in figure 7(a). For all of the values of G , the growth rate follows a similar spatial pattern. First, near the flame, a_r is small or zero and then steeply rises near $y = y_1$. Then, a_r is basically constant or slightly increasing until $y = y_2$. We refer to this area of constant a_r as the ‘plateau region’. Physically, the plateau region is the area in which the Landau equation holds. This means that the plateau region organizes the entire flow and represents the region of absolute instability. For larger values of y , a_r rises steeply again. For these large values of y , the measurement of a_r is not very accurate because u_x saturates quickly. In general, there was little dependence of the calculated Landau constants on x , and so all constants were averaged in the x direction for a given y . We used the criterion that at least 25% of points in the x direction must have had their u_x time series successfully fitted by the fitting algorithm for an average value to be calculated. By doing so, we implicitly assumed that the plateau region was rectangular to first order. The percentage value chosen did not make a substantial difference to the Landau constants, although it did affect the location of y_1 to some extent.

To calculate the representative a_r value for a given G , we averaged a_r on the plateau between $y = y_1$ and $y = y_2$. These results are shown in figure 7(b). The growth rate scales as $(G - G_{cr})$, as predicted by (4.6b), up to somewhere between $G = 0.27$ and $G = 0.28$. At this point, we have left the regime near G_{cr} where the Landau equation and a Taylor expansion of the Landau constants are valid.

To infer G_{cr} , we used a linear fit of the first four points in figure 7(b) to find the G for which $a_r = 0$. This is, by definition, G_{cr} , the value of G for which the instability begins. Specifically, we found that $G_{cr} = 0.2178$. We expect this result to be accurate to approximately ± 0.005 , so that G_{cr} lies roughly between 0.21 and 0.22. We also measured da_r/dG and found $da_r/dG = 0.0776$.

The plateau region moves closer to the flame front for higher values of G (see figures 4 and 5). For $G \geq 0.3$, the unstable area disturbs the flame front itself, which causes the pulsations observed by Vladimirova & Rosner (2005).

Next, we measured the saturated velocity as a function of y for different values of G ; the results are shown in figure 8. The saturated velocity was unmeasurable where

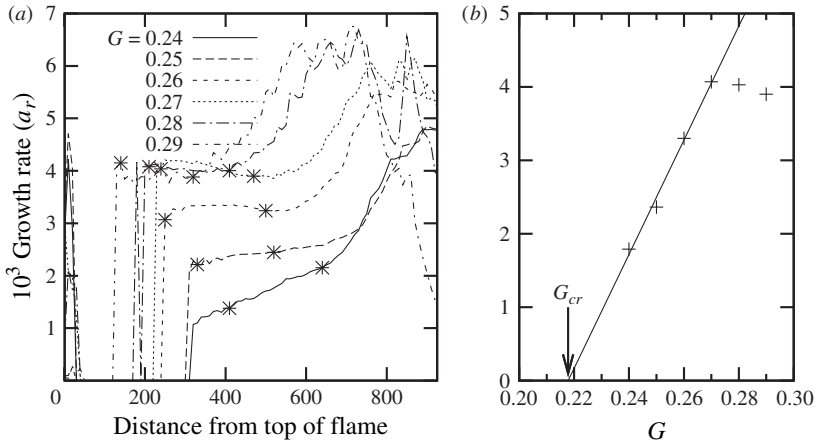


FIGURE 7. (a) The growth rate. Here, y is the distance from the top of flame. The star points represent the boundaries, $y = y_1$ and $y = y_2$, of the plateau used to average over a_r . The plateau is the region of absolute instability in which the Landau equation holds. Measurements of a_r become inaccurate for y much larger than y_2 , because the instability saturates almost immediately. There is some unphysical noise in the measurements of a_r for $y < y_1$ and y_1 is somewhat dependent on the number of points required to calculate an average in the x direction. (b) A plot of a_r versus G . This figure shows the linear relationship between the growth rate and G . For $G = 0.28$ and $G = 0.29$ this relationship no longer holds. Extrapolation back to $a_r = 0$ gives $G_{cr} = 0.2178$. We expect this result to be accurate to approximately ± 0.005 , so that G_{cr} lies roughly between 0.21 and 0.22.

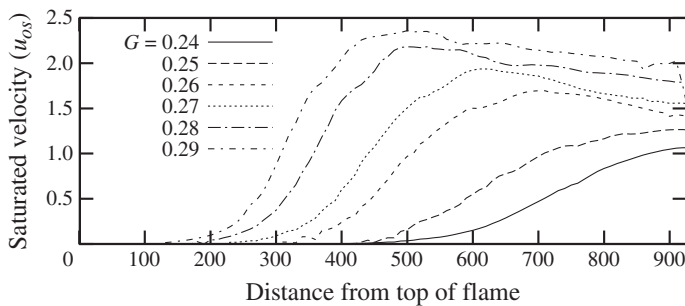


FIGURE 8. The saturated velocity shown as a function of the distance from the top of the flame. A zero value of u_{os} indicates either no instability or an inability to measure u_{os} accurately.

this plot shows $u_{os} = 0$. There was either actually no growth of the instability, or the instability grew, but the deviation from exponential growth for a_r was so small (over the time of the simulation) that the saturated velocity could not be measured. In general, whenever $a_r > 0$, u_{os} should also be non-zero.

The saturated velocity is small, or zero, near the flame front and gets larger as the distance from the flame increases. At a certain point, $y = y_{max}$, the saturated velocity reaches a maximum and thereafter declines. This decline is due to viscous dissipation between the horizontal shear layers which removes energy from the system. As was the case with a_r , the area where u_{os} becomes non-negligible moves closer to the flame front for higher values of G and a higher maximum value of u_{os} is reached.

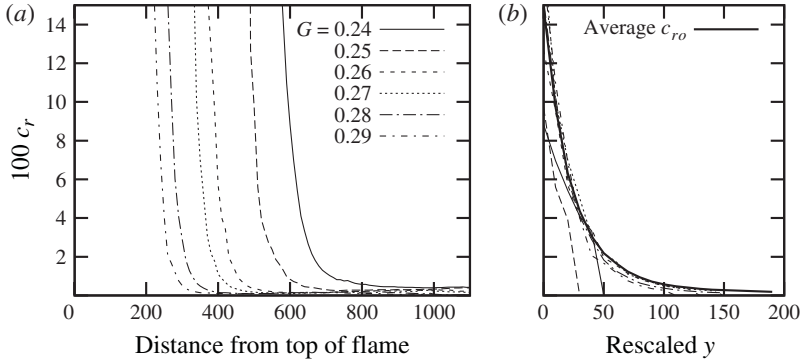


FIGURE 9. (a) The saturation factor c_r as a function of distance from the top of the flame. (b) The collapse of the c_r curves. This figure shows the curves from (a) shifted to overlap as well as possible.

G	y_1	y_{cr}	y_2	y_{max}
0.24	410	530	640	870
0.25	330	410	520	730
0.26	250	340	500	590
0.27	240	300	470	530
0.28	210	260	410	540
0.29	140	220	320	500

TABLE 1. Key distances from the top of the flame. The a_r plateau region begins at y_1 . Here, y_{cr} is the y value at which $u_{os} = 0.15$. The a_r plateau ends at y_2 . The saturated velocity, u_{os} , reaches a maximum at y_{max} .

Using the measurements of a_r and u_{os} , we calculated c_r from (4.6e). The result is shown in figure 9(a). Here, c_r is the only Landau constant that varies in space in the plateau region. It must vary because the saturation velocity grows with distance from the flame front. The spatial dependence of c_r is the ‘secondary spatial dependence’ of the Landau equation.

The next question is whether or not $dc_r/dG = 0$, but our answer here is speculative. Graphically, the issue is whether the c_r curves collapse onto a single master curve when the plateau regions are lined up perfectly. The curves superficially have the same shape (see figure 9a). In figure 9(b), we show a ‘collapse’ of the c_r curves when the plateau zones are lined up using $y = y_{cr}$ (see table 1). Visually, the curves seem to collapse to first order, but the error in measuring u_{os} , especially for the lower G values, is too large to know for sure. Also, the measurement grid resolution of 10 physical units in the y -direction limits how well the curves can be shifted on top of one another. We are inclined to think that if the fitting of u_{os} could be improved for low values of G then the curves would fully collapse; however, we cannot confirm this on the basis of our current data in spite of the suggestive similarity of the curves in figure 9(a).

Because of our uncertainty about the value of dc_r/dG , we now briefly explore the effect of a possibly non-zero value. In the derivation of (4.6c) from (4.5c), we assumed that $dc_r/dG \approx 0$. Even if this is not the case, equation (4.5c) could still take on the approximate form (4.6c) if the second term were not zero but merely much

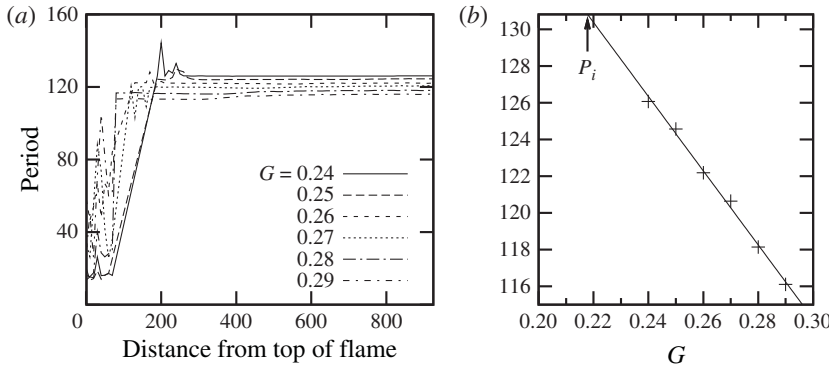


FIGURE 10. (a) The period of the oscillations of u_x as a function of the distance from the top of the flame. The data for low values of y are probably unphysical. (b) The oscillation period versus G . This figure shows the linear relationship between the oscillation period and G . Extrapolation back to $G_{cr} = 0.2178$ gives $P_i = 130.82$.

smaller than the first term. In fact, if $dc_r/dG > 0$, then the first term will always be larger than the second term for finite values of dc_r/dG . If $dc_r/dG < 0$, then the singularity in the denominator of the second term could cause it to diverge so that the second term would have to be taken into account as the dominant term. This case seems less likely because if $dc_r/dG < 0$ then c_r could become negative, leading to superexponential growth of u_o , which is physically unlikely. Therefore, the effect of a non-zero dc_r/dG depends on its sign. If $dc_r/dG > 0$, which is likely, then the use of (4.6c) is still justified.

The final measurement is of the period of oscillations, P , from which we find a_{io} and da_i/dG . Figure 10(a) shows the dependence of the period of the oscillations of u_x on the distance from the flame front. Close to the flame front, the period seems to vary quite a bit. These measurements are probably not physically meaningful because a_r and u_o are practically zero in this region. In the plateau region and downstream of the plateau region the period is completely constant. The oscillations of u_x are completely dominated by one pure frequency, exactly as is expected for a flow dominated by a region of absolute instability. By extrapolating back to G_{cr} , we find that the initial period of the bifurcation is $P_i = 130.82$ (see figure 10b). A finite value for the initial period supports the idea that the bifurcation at G_{cr} is a Hopf bifurcation. The period and dP/dG can be used to find $a_{io} = 0.0475$ and $da_i/dG = 0.0918$. We also found that the frequency of the oscillations does not vary with time, so $c_{io} = 0$ and $dc_{io}/dG = 0$.

The Landau constants derived from our simulations are given in table 2. All of the constants are independent of y except for c_m , which has the form shown in figure 9(a). The Landau equations become

$$\frac{du_o}{dt} = 0.0776(G - 0.2178)u_o - c_r(y)u_o^3, \tag{5.3a}$$

$$\frac{d\phi}{dt} = 0.0475 + 0.0918(G - 0.2178). \tag{5.3b}$$

These equations are a simple temporal evolution model for u_x within the plateau region. They are relevant for values of $G \geq G_{cr}$ within the neighbourhood of G_{cr} in which the Taylor series expansion is applicable.

G_{cr}	da_r/dG	a_{io}	da_i/dG	c_{ro}	dc_r/dG	c_{io}	dc_i/dG
0.2178	0.0776	0.0475	0.0918	$c_{ro}(y)$	$\approx 0(?)$	0	0

TABLE 2. The values of the Landau constants as calculated from our simulations. It should be noted that only c_{ro} depends on position. In terms of period, these constants translate to $P_i = 130.82$ and $dP/dG = 174.82$, so that $P = 130.82 - 174.82(G - G_{cr})$.

6. Discussion

In the previous section, we showed that the shear instability of the vorticity rolls downstream of the flame front, seen when G is near G_{cr} , can be described by the Landau equation, with u_x as the amplitude parameter. As the instability begins, the oscillations of u_x grow exponentially with a growth rate a_r until they saturate to a maximum amplitude $u_{os}(y)$ because of nonlinear effects, controlled by $c_{ro}(y)$. The period of the oscillations of u_x , given by a_{io} , does not change with time (because $c_i = 0$) but does get shorter as G increases because $da_i/dG > 0$. The instability begins at a critical value of $G_{cr} = 0.2178$, or between $G = 0.21$ and 0.22 with our expected accuracy. The Landau equation is a good model up to approximately $G = 0.28$ when multiple modes of the instability begin to interact. This interaction stops the linear growth of a_r with G , but, interestingly, does not affect the linear decrease of the period of oscillation with G . Spatially, the instability takes place in a ‘plateau region’ in which the growth rate, a_r , is constant. We suggested that this plateau region is, in fact, a region of absolute instability that controls the flow. Within the plateau region, the only spatial dependence is of c_{ro} and therefore of the saturated velocity, u_{os} ; this is the secondary spatial dependence of the Landau equation. Otherwise, the growth of the instability is entirely temporal. Overall, we found that the Landau equation models the shear instability downstream of the flame front, just as it models the shear instability downstream of a circular cylinder.

Since the flame system follows the Landau equation, it may undergo a Hopf bifurcation at G_{cr} , that is, a change from steady behaviour ($u_x = 0$) to periodic behaviour (u_x oscillates). The Landau equation implies a Hopf bifurcation, under certain circumstances, because it matches the normal form of the Hopf bifurcation with added constants. That normal form is (Marsden & McCracken 1976; Sprott 2003)

$$\frac{dr}{dt} = r(\mu - r^2), \quad (6.1a)$$

$$\frac{d\phi}{dt} = 1. \quad (6.1b)$$

Here, r is the radius of the limit cycle and ϕ is the phase. The Landau equation matches this normal form (adding constants in front of the normal form terms) if c_r and a_i in (4.2b) are constants and $c_i = 0$. Here, $\mu = a_r$ plays the role of the control parameter. If c_r and a_i are not constant, then there are three control parameters instead of one and the bifurcation structure is more complicated. However, as long as c_r and a_i do not change sign, the bifurcation is still a simple Hopf bifurcation. This turns out to be the case; a_i decreases with G , but the period cannot become negative. Therefore, the angular frequency of the limit cycle varies as G changes but the bifurcation type (Hopf) is unchanged. We found that c_r is probably constant, but if it were not then the

radius of the limit cycle would just vary in a different way from the standard Hopf bifurcation. In fact, c_r is unlikely to change sign because then the growth of u_x would be superexponential. If it is true that $dc_r/dG = 0$, then (4.5c) becomes (4.6c) and u_{os} takes on the particularly nice dependence that $u_{os} \propto (G - G_{cr})^{1/2}$. This is the typical amplitude dependence that is seen with the simplest form of the Hopf bifurcation.

In the complex plane of eigenvalues, a Hopf bifurcation corresponds to a pair of complex conjugate eigenvalues crossing from the negative real half of the plane to the positive real half of the plane at non-zero speed and with a non-zero imaginary part. In practice, this means that the oscillations must appear with a ‘finite’ (non-infinite) period and that da_r/dG must be greater than zero. Both of these requirements are fulfilled here; we found that $P_i = 130.82$ and $da_r/dG = 0.0776$. Sreenivasan *et al.* (1987) showed that these requirements are also fulfilled for the cylinder case – the onset of the instability for both the cylinder and flame is a Hopf bifurcation.

Finally, we speculate that the shear instability is controlled by an absolute instability. We reason by analogy with the case of flow past a cylinder, for which Strykowski (1986), Sreenivasan *et al.* (1987) and Strykowski & Sreenivasan (1990) introduced several pieces of evidence to support the idea that an absolute instability controls the wake. First, and most importantly, the cylinder wake is dominated by pure frequency oscillations. This signifies an absolute instability because the resonance mechanism amplifies one frequency (Huerre & Monkewitz 1985; Koch 1985; Monkewitz & Nguyen 1987). Convective instabilities, on the other hand, tend to show broadband noise. We showed that the flame wake is also dominated by pure frequencies in § 5.2. Second, Strykowski and Sreenivasan argued that the fact that the wake can be modelled by the Landau equation, with only secondary spatial dependences, supports the absolute instability model. We also showed that this was the case for the flame wake. As the final evidence suggesting a region of absolute instability, Strykowski and Sreenivasan showed that, by adding a small secondary cylinder to the flow, the vortex street can be suppressed for certain values of Re . The second cylinder suppresses the resonance and disrupts the feedback process, destroying the growth of the instability. This behaviour is plausible only for a region controlled by an absolute instability. We suggest that the reflecting walls of the flame simulations in Vladimirova & Rosner (2003) might have acted to suppress feedback in a similar fashion.

In conclusion, we find that the low-gravity pulsations observed by Vladimirova & Rosner (2005) are not due to an innate instability of the flame front, but to the interaction of the flame front with an instability of the shear layers downstream of the flame front. This instability is controlled by a region of absolute instability located downstream of the flame front and is well-described by the Landau equation. The onset of the instability is a Hopf bifurcation. The instability is analogous to the instability of the shear layers downstream of a circular cylinder. When the region of absolute instability is far enough away from the flame front, the flame front does not pulsate, and the travelling wave solution for the flame is stable (not metastable as postulated by Vladimirova & Rosner 2005). For larger values of G , the region of absolute instability moves closer to the flame front, until finally it is close enough to interact with the flame and cause flame pulsations. Overall, the flame and its shear instability are an excellent demonstration of the fact that a solid body is not needed to create a vortex street (Abernathy & Kronauer 1962; Gerrard 1966; Strykowski & Sreenivasan 1990). In the case of the cylinder, the solid body functions only to create the shear layers downstream of the cylinder, which then drive the instability. In the same way, the flame merely creates the rolls which then become unstable and drive vortex shedding. In the low- G regime, burning and gravity are secondary concerns; it is the self-generated flow behind the flame that controls the behaviour of the flame.

The aim of this paper was to determine why different flame morphologies are seen for different kinds of boundary conditions. Impermeable/adiabatic boundary conditions result in metastable and stable parabolic solutions; reflecting boundary conditions result in stable parabolic solutions with cusps; however, periodic boundary conditions result in unstable, pulsating flames. In this paper, we showed that the flame pulsations are due to an interaction between the flame front and an instability of the shear layers downstream from the flame front. This explains why RT unstable flame simulations for the Type Ia supernova problem, which use periodic boundary conditions, inevitably see complex flame morphologies, but experiments and simulations of flames in confined scenarios see simple, stable flame shapes. We suggest that impermeable/adiabatic or reflecting boundary conditions suppress feedback in the region of absolute instability downstream of the flame front, while periodic boundary conditions do not, allowing the shear instability to develop. This suggests that this instability may operate in unconfined domains because the instability downstream of a cylinder is unconfined, and we have shown that the development of the shear instability downstream of the flame is governed by the same equations. Of course, a complete analysis of the unconfined dynamics of RT unstable flames must also take into account the unsaturated growth of the RT instability. However, as shown in this paper, when RT unstable flames produce shear layers the instability of these layers can interact with the flame front. Therefore, a full analysis of unconfined RT unstable flames must include both the deformation of the flame front by the RT instability and the interaction of shear layer instabilities with the flame front.

Acknowledgements

I would like to thank my thesis adviser, Robert Rosner, for all of his advice and support. I also thank the other members of my thesis committee, A. Königl, F. Cattaneo and A. Olinto, for their advice and insight into this research. I am grateful to P. Fischer and A. Obabko for making Nek5000 available and for giving me advice on using the code and to N. Vladimirova for useful discussions on flames in general and for introducing me to the code and providing scripts when I first started working on this problem. I am also very grateful to S. Abarzhi for advice on the Landau equation. I would like to thank T. Venters, J. Johnsen and S. Teitler for useful discussions. This paper greatly benefitted from proofreading by and content suggestions from P. Flath, S. Tarzia and T. Venters. I would also like to thank the anonymous referees and the Editor, Professor Moshe Matalon, for useful and thought-provoking questions, comments and suggestions. This research used resources of the National Energy Research Scientific Computing Center (NERSC), which is supported by the Office of Science of the US Department of Energy under contract no. DE-AC02-05CH11231.

REFERENCES

- ABERNATHY, F. H. & KRONAUER, R. E. 1962 The formation of vortex streets. *J. Fluid Mech.* **13** (1), 1–20.
- BELL, J. B., DAY, M. S., RENDLEMAN, C. A., WOOSLEY, S. E. & ZINGALE, M. 2004 Direct numerical simulations of Type Ia supernovae flames. II. The Rayleigh–Taylor instability. *Astrophys. J.* **608**, 883–906.
- BERESTYCKI, H., KAGAN, L., KAMIN, S. & SIVASHINSKY, G. I. 2004 Metastable behavior of premixed gas flames in rectangular channels. *Interfaces Free Bound.* **6**, 423–438.

- BERESTYCKI, H., KAMIN, S. & SIVASHINSKY, G. I. 1995 Nonlinear dynamics and metastability in a Burgers type equation (for upward propagating flames). *C. R. Acad. Sci. Paris I* **321**, 185–190.
- BERESTYCKI, H., KAMIN, S. & SIVASHINSKY, G. I. 2001 Metastability in a flame front evolution equation. *Interfaces Free Bound.* **3** (4), 361–392.
- BYCHKOV, V. V., GOLBERG, S. M., LIBERMAN, M. A. & ERIKSSON, L. E. 1996 Propagation of curved stationary flames in tubes. *Phys. Rev. E* **54**, 3713–3724.
- BYCHKOV, V. V. & LIBERMAN, M. A. 2000 Dynamics and stability of premixed flames. *Phys. Rep.* **325**, 115–237.
- CHERTKOV, M., LEBEDEV, V. & VLADIMIROVA, N. 2009 Reactive Rayleigh–Taylor turbulence. *J. Fluid Mech.* **633**, 1–16.
- CHEVIAKOV, A. F. & WARD, M. J. 2007 A two-dimensional metastable flame-front and degenerate spike-layer problem. *Interfaces Free Bound.* **9**, 513–547.
- CLAVIN, P. & WILLIAMS, F. A. 1982 Effects of molecular diffusion and of thermal expansion on the structure and dynamics of premixed flames in turbulent flows of large scale and low intensity. *J. Fluid Mech.* **116**, 251–282.
- CONSTANTIN, P., KISELEV, A. & RYZHIK, L. 2003 Fronts in reactive convection: bounds, stability, and instability. *Commun. Pure Appl. Maths* **56** (12), 1781–1803.
- CRETA, F. & MATALON, M. 2011 Strain rate effects on the nonlinear development of hydrodynamically unstable flames. *Proc. Combust. Inst.* **33** (1), 1087–1094.
- DAMKOHLER, G. 1940 (trans. 1947) Der Einfluss der Turbulenz auf die Flammgeschwindigkeit in Gasgemischen (English Translation: the effects of turbulence on the flame velocity in gas mixtures). *Z. Elektrochem.* **46** (trans. 1112), 601–626; (trans. in Technical memorandums. United States. National Advisory Committee for Aeronautics) (trans. 1–51).
- DARRIEUS, G. 1938 Propagation d'un front de flamme. Unpublished Work, Presented at La Technique Moderne (Paris), and in 1945 at Congrès de Mécanique Appliquée (Paris).
- DRAZIN, P. G. & REID, W. H. 2004 *Hydrodynamic Stability*. 2nd edn Cambridge University Press.
- FISCHER, P. F., LOTTES, J. W. & KERKEMEIER, S. G. 2008 Nek5000 Web Page. <http://nek5000.mcs.anl.gov>.
- GERRARD, J. H. 1966 The mechanics of the formation region of vortices behind bluff bodies. *J. Fluid Mech.* **25** (2), 401–413.
- GUIDI, L. F. & MARCHETTI, D. H. U. 2003 A comparison analysis of Sivashinsky's type evolution equations describing flame propagation in channels. *Phys. Lett. A* **308** (2–3), 162–172.
- HICKS, E. P. & ROSNER, ROBERT. 2013 Gravitationally unstable flames: Rayleigh–Taylor stretching versus turbulent wrinkling. *Astrophys. J.* **771** (2), 135.
- HUERRE, P. & MONKEWITZ, P. A. 1985 Absolute and convective instabilities in free shear layers. *J. Fluid Mech.* **159**, 151–168.
- KAMIN, S., BERESTYCKI, H., KAGAN, L. & SIVASHINSKY, G. I. 2005 Metastable behavior of premixed gas flames. *Progr. Nonlinear Differential Equations Appl.* **630**, 319–328.
- KHOKHLOV, A. M. 1995 Propagation of turbulent flames in supernovae. *Astrophys. J.* **449**, 695–713.
- KOCH, W. 1985 Local instability characteristics and frequency determination of self-excited wake flows. *J. Sound Vib.* **99** (1), 53–83.
- LANDAU, L. D. 1944 On the theory of slow combustion. *Acta Physicochim. USSR* **19**, 17–85.
- LANDAU, L. D. & LIFSHITZ, E. M. 2004 *Fluid Mechanics*, 2nd edn, Course of Theoretical Physics, vol. 6 Elsevier Science Ltd.
- MARKSTEIN, G. H. (Ed.) 1964 *Non-Steady Flame Propagation*, The Macmillan Company.
- MARSDEN, JEROLD. E. & MCCracken, M. 1976 *The Hopf Bifurcation and its Applications*. Springer.
- MATALON, M. 2007 Intrinsic flame instabilities in premixed and nonpremixed combustion. *Annu. Rev. Fluid Mech.* **391**, 163–191.
- MATALON, M., CUI, C. & BECHTOLD, J. K. 2003 Hydrodynamic theory of premixed flames: effects of stoichiometry, variable transport coefficients and arbitrary reaction orders. *J. Fluid Mech.* **487**, 179–210.
- MATALON, M. & MATKOWSKY, B. J. 1982 Flames as gasdynamic discontinuities. *J. Fluid Mech.* **124**, 239–259.

- MICHELSON, D. M. & SIVASHINSKY, G. I. 1977 Nonlinear analysis of hydrodynamic instability in laminar flames – II. Numerical experiments. *Acta Astronaut.* **4** (11–12), 1207–1221.
- MIKISHV, A. B. & SIVASHINSKY, G. I. 1993 Quasi-equilibrium in upward propagating flames. *Phys. Lett. A* **175** (6), 409–414.
- MONKEWITZ, P. A. & NGUYEN, L. N. 1987 Absolute instability in the near-wake of two-dimensional bluff bodies. *J. Fluids Struct.* **1** (2), 165–184.
- OU, C. & WARD, M. J. 2006 A metastable flame-front interface and Carrier’s problem. *J. Comput. Appl. Maths* **190** (1–2), 354–375.
- PELCE, P. & CLAVIN, P. 1982 Influence of hydrodynamics and diffusion upon the stability limits of laminar premixed flames. *J. Fluid Mech.* **124**, 219–237.
- PROVANSAL, M., MATHIS, C. & BOYER, L. 1987 Bénard–von Kármán instability: transient and forced regimes. *J. Fluid Mech.* **182**, 1–22.
- RAKIB, Z. & SIVASHINSKY, G. I. 1987 Instabilities in upward propagating flames. *Combust. Sci. Technol.* **54**, 69–84.
- RASTIGEJEV, Y. & MATALON, M. 2006 Nonlinear evolution of hydrodynamically unstable premixed flames. *J. Fluid Mech.* **554**, 371–392.
- RAYLEIGH, LORD 1883 Investigation of the character of the equilibrium of an incompressible heavy fluid of variable density. *Proc. Lond. Math. Soc.* **14**, 170–177.
- SIVASHINSKY, G. I. 1977 Nonlinear analysis of hydrodynamic instability in laminar flames – I. Derivation of basic equations. *Acta Astronaut.* **4** (11–12), 1177–1206.
- SPROTT, J. C. 2003 *Chaos and Time-Series Analysis*. Oxford University Press.
- SREENIVASAN, K. R., STRYKOWSKI, P. J. & OLINGER, D. J. 1987 Hopf bifurcation, Landau equation, and vortex shedding behind circular cylinders. In *Forum on Unsteady Flow Separation* (ed. K. N. Ghia), pp. 1–13. ASME.
- STRYKOWSKI, P. J. 1986 The control of absolutely and convectively unstable flows. PhD thesis, Yale University.
- STRYKOWSKI, P. J. & SREENIVASAN, K. R. 1990 On the formation and suppression of vortex ‘shedding’ at low Reynolds numbers. *J. Fluid Mech.* **218**, 71–107.
- SUN, X. & WARD, M. J. 1999 Metastability for a generalized Burgers equation with applications to propagating flame fronts. *Eur. J. Appl. Maths* **10**, 27–53.
- TAYLOR, G. 1950 The instability of liquid surfaces when accelerated in a direction perpendicular to their planes. I. *Proc. R. Soc. Lond. A* **201**, 192–196.
- THUAL, O., FRISCH, U. & HÉNON, M. 1985 Application of pole decomposition to an equation governing the dynamics of wrinkled flame fronts. *J. Physique* **46**, 1485–1494.
- VAYNBLAT, D. & MATALON, M. 2000a Stability of pole solutions for planar propagating flames: I. Exact eigenvalues and eigenfunctions. *SIAM J. Appl. Maths* **60** (2), 679–702.
- VAYNBLAT, D. & MATALON, M. 2000b Stability of pole solutions for planar propagating flames: II. Properties of eigenvalues/eigenfunctions and implications to stability. *SIAM J. Appl. Maths* **60** (2), 703–728.
- VLADIMIROVA, N. & ROSNER, R. 2003 Model flames in the Boussinesq limit: the effects of feedback. *Phys. Rev. E* **67** (6), 066305.
- VLADIMIROVA, N. & ROSNER, R. 2005 Model flames in the Boussinesq limit: the case of pulsating fronts. *Phys. Rev. E* **71** (6), 067303.
- VLADIMIROVA, N., WEIRS, V. G. & RYZHIK, L. 2006 Flame capturing with an advection–reaction–diffusion model. *Combust. Theor. Model.* **10** (4), 727–747.
- XIN, J. 2000 Front propagation in heterogeneous media. *SIAM Rev.* **42** (2), 161–230.
- ZELDOVICH, YA. B., BARENBLATT, G. I., LIBROVICH, V. B. & MAKHVILADZE, G. M. 1985 *The Mathematical Theory of Combustion and Explosions*. Consultants Bureau.
- ZHANG, J., BRONSON MESSER, O. E., KHOKHLOV, A. M. & PLEWA, T. 2007 On the evolution of thermonuclear flames on large scales. *Astrophys. J.* **656**, 347–365.
- ZINGALE, M., WOOSLEY, S. E., RENDLEMAN, C. A., DAY, M. S. & BELL, J. B. 2005 Three-dimensional numerical simulations of Rayleigh–Taylor unstable flames in Type Ia supernovae. *Astrophys. J.* **632**, 1021–1034.